Transmembrane location of retinal in bacteriorhodopsin by neutron diffraction

5 AUTHORS, INCLUDING:

Harald Otto
Freie Universität Berlin
53 PUBLICATIONS   **1,763** CITATIONS

SEE PROFILE

Josef Westerhausen
Deutsche Gesellschaft für Lebensmittelsicher…
8 PUBLICATIONS   **204** CITATIONS

SEE PROFILE

Maarten P Heyn
Freie Universität Berlin
119 PUBLICATIONS   **4,995** CITATIONS

SEE PROFILE

Park, M. H., Yamamoto, T., & Nakanishi, K. (1989) *J. Am. Chem. Soc. 111*, 4997–4998.

Scherrer, P., & Stoeckenius, W. (1984) *Biochemistry 23*, 6195–6202.

Seiff, F., Wallat, I., Westerhausen, J., & Heyn, M. P. (1986) *Biophys. J. 50*, 629–635.

Sen, R., Widlanski, T. S., Balogh-Nair, V., & Nakanishi, K. (1982) *J. Am. Chem. Soc. 105*, 5160–5162.

Sheves, M., Baasov, T., Friedman, N., Ottolenghi, M., Feinmann-Weinberg, R., Rosenbach, V., & Ehrenberg, B. (1984) *J. Am. Chem. Soc. 106*, 2435–2437.

Stoeckenius, W., & Bogomolni, R. A. (1982) *Annu. Rev. Biochem. 52*, 587–616.

Stoeckenius, W., Lozier, R. H., & Bogomolni, R. A. (1979) *Biochim. Biophys. Acta 505*, 215–278.

Swank, R. T., & Munkres, K. D. (1971) *Anal. Biochem. 39*, 462–477.

Tarr, G. E., & Crabb, J. W. (1983) *Anal. Biochem. 131*, 99–107.

Trewhella, J., Anderson, S., Fox, R., Gogol, E., Khan, S., Engelman, D. M., & Zaccai, G. (1983) *Biophys. J. 42*, 233–241.

Trewhella, J., Popot, J.-L., Zaccai, G., & Engelman, D. (1986) *EMBO J. 5*, 3045–3049.

Wallace, B. A., & Henderson, R. (1982) *Biophys. J. 39*, 233–239.

Transmembrane Location of Retinal in Bacteriorhodopsin by Neutron Diffraction[†]

T. Hauss, S. Grzesiek, H. Otto, J. Westerhausen, and M. P. Heyn*

Biophysics Group, Department of Physics, Freie Universität Berlin, Arnimallee 14, D-1000 Berlin 33, Federal Republic of Germany

Received July 25, 1989; Revised Manuscript Received December 8, 1989

ABSTRACT: The transmembrane location of the chromophore of bacteriorhodopsin was obtained by neutron diffraction on oriented stacks of purple membranes. Two selectively deuterated retinals were synthesized and incorporated in bacteriorhodopsin by using the retinal⁻ mutant JW5: retinal-d_{11} (D11) contained 11 deuterons in the cyclohexene ring, and retinal-d_5 (D5) had 5 deuterons as close as possible to the Schiff base end of the chromophore. The membrane stacks had a lamellar spacing of 53.1 Å at 86% relative humidity. Five orders were observed in the lamellar diffraction pattern of the D11, D5, and nondeuterated reference samples. The reflections were phased by D_2O–H_2O exchange. The absolute values of the structure factors were nonlinear functions of the D_2O content, suggesting that the coherently scattering domains consisted of asymmetric membrane stacks. The centers of deuteration were determined from the observed intensity differences between labeled and unlabeled samples by using model calculations and Fourier difference methods. With the origin of the coordinate system defined midway between consecutive intermembrane water layers, the coordinates of the center of deuteration of the D11 and D5 label are 10.5 ± 1.2 and 3.8 ± 1.5 Å, respectively. Alternatively, the label distance may be measured from the nearest membrane surface as defined by the maximum in the neutron scattering length density at the water/membrane interface. With respect to this point, the D11 and D5 labels are located at a depth of 9.9 ± 1.2 and 16.6 ± 1.5 Å, respectively. The chromophore is tilted with the Schiff base near the middle of the membrane and the ring closer to the membrane surface. The vector connecting the two label positions in the chromophore makes an angle of 40 ± 12° with the plane of the membrane. Of the two possible orientations of the plane of the chromophore, which is perpendicular to the membrane plane, only the one in which the N→H bond of the Schiff base points toward the same membrane surface as the vector from the Schiff base to the cyclohexene ring is compatible with the known tilt angle of the polyene chain.

Bacteriorhodopsin (BR)[1] is a membrane-bound protein from *Halobacterium halobium* which functions as a light-driven proton pump. The primary event of absorption occurs at the chromophore, which consists of retinal bound via a protonated Schiff base to lysine 216. Following absorption, a photocycle takes place in which the pigment goes through several spectral intermediates before returning to the ground state in about 10 ms. During the first part of the cycle the Schiff base is deprotonated and a proton is released to the extracellular medium. In the course of the second part a proton is taken up from the cytoplasm and the Schiff base is reprotonated. Recent optical and electrical measurements show that one proton is translocated per cycle (Drachev et al., 1984; Grzesiek & Dencher, 1986; Braun et al., 1988; Kouyama et al., 1988b), making it very likely that the Schiff base proton is directly involved in the proton translocation. Associated with the photocycle is a cyclic trans–cis isomerization at the 13–14 double bond of the chromophore. The interaction of the chromophore with charges in the protein environment and the protonation state of the Schiff base are the main factors involved in the color regulation of the pigment. In all of these

[1] Abbreviations: PM, purple membrane; BR, bacteriorhodopsin; Pro-BR, D5-BR, and D11-BR, BR regenerated with native retinal, retinal-d_5, and retinal-d_{11}, respectively; D5, retinal-d_5; D11, retinal-d_{11}.
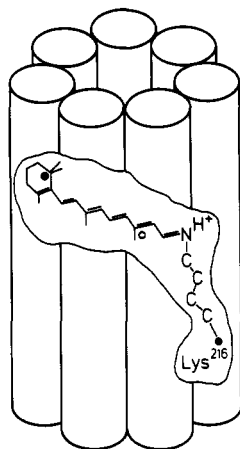
FIGURE 1: Transmembrane position of the retinal chromophore of BR—an artist's view. (●, ○) Approximate positions of the centers of deuteration of the two labeled retinals used in this study (see Figure 2). The line connecting these two points makes an angle of about 15° with the polyene chain.
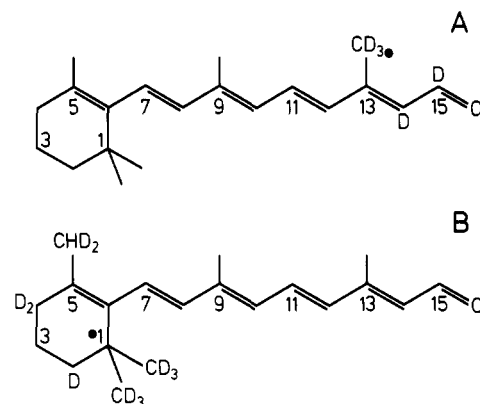

FIGURE 2: Specifically deuterated retinals. The chemical structure of the synthetic retinals was determined by ^1H NMR and mass spectroscopy. (●) Approximate position of the center of deuteration for the respective label (calculated as the center of mass of the deuterons). (A) Retinal-d_5. (B) Retinal-d_{11}.

aspects concerning the function and properties of bacteriorhodopsin, the chromophore plays a central role and structural information on its position is clearly of considerable importance. In particular, models for the mechanism of proton translocation must take into account the distances between putative donor and acceptor groups and the Schiff base.

The structure of the two-dimensional purple membrane (PM) lattice projected onto the plane of the membrane has been determined to a resolution of 2.8 Å (Baldwin et al., 1988). In the density maps the chromophore could not be resolved, however. Its in-plane location was recently determined by using neutron diffraction with selectively deuterated retinals (Seiff et al., 1985, 1986; Heyn et al., 1988). Contradictory results were obtained for the transmembrane depth. A cartoon of the arrangement of the chromophore within bacteriorhodopsin is shown in Figure 1. Neutron diffraction experiments with perdeuterated retinal placed the chromophore close to the middle of the membrane (King et al., 1979). Fluorescence energy transfer experiments, on the other hand, indicated that the chromophore is at a depth of about 10 Å from the cytoplasmic side of the membrane (Kouyama et al., 1988a; Otomo et al., 1988; Tsetlin et al., 1983). On the basis of surface-enhanced resonance Raman experiments, it was concluded that the chromophore is only 6 Å away from the extracellular surface (Nabiev et al., 1985). Photoaffinity (Huang et al., 1982) and time-resolved electrical measurements (Keszthelyi & Ormos, 1980; Holz et al., 1988) also suggested an asymmetric location with the chromophore closer to the extracellular surface.

We have used lamellar neutron diffraction on oriented multilayers of purple membranes with partially deuterated retinals to determine the transmembrane location of both ends of the chromophore separately. The labeled retinals were incorporated in purple membrane by using a mutant that is deficient in the synthesis of retinal (Seiff et al., 1985). For one of the retinals the deuteration was concentrated in the cyclohexene ring; for the other the label was as close as possible to the Schiff base (see Figure 2). The difference in scattering length between deuterated and nondeuterated retinal leads to differences in the diffraction intensities, from which the center of deuteration may be evaluated by model calculations and Fourier difference methods.

For the mechanism of the proton pump, it is of particular importance to know the depth of the Schiff base and the direction of the Schiff base N→H bond vector. Linear di-

chroism experiments indicate that the polyene chain of the chromophore is tilted by about 20° with respect to the plane of the membrane (Heyn et al., 1977; Bogomolni et al., 1977). The plane of the chromophore itself is thought to be perpendicular to the membrane (Earnest et al., 1986; Ikegami et al., 1987; Heyn et al., 1988). Only two possibilities therefore exist for the orientation of the retinal plane, the one depicted in Figure 1 and that obtained from it by rotating the chromophore over π around the polyene chain. Since the vector connecting the two centers of deuteration in our two retinals makes an angle of 15° with the polyene chain (see also Figure 2), its angle with respect to the plane of the membrane should be either ≈5° or ≈35°. The difference of 30° is expected to be sufficient to distinguish between the two orientations in our experiment.

MATERIALS AND METHODS

Sample Preparation. Two specifically deuterated retinals were synthesized and characterized as described earlier (Heyn et al., 1988; Seiff et al., 1986). The first one (D5) has the 5 protons nearest to the chain end replaced by deuterons (Figure 2A), and the other (D11) has 11 protons in the cyclohexene ring replaced by deuterons (Figure 2B). Regeneration of retinal⁻ mutants (strain JW5) by fully protonated retinal and retinal-d_5 and -d_{11} was performed as described (Seiff et al., 1985). For each sample 150 mg of purple membrane suspended in deionized water was applied to both sides of 10 quartz slides of 0.3-mm thickness on an area of 25 × 10 mm² and dried slowly (≥72 h) at controlled humidity (≥80%). In this way samples suitable for lamellar diffraction were obtained with the purple membranes arranged in stacks and oriented parallel to the quartz support. In order to obtain identical humidity and temperature conditions for the three samples containing fully protonated (Pro) retinal and retinal-d_{11} and -d_5, they were mounted vertically along the diffractometer axis in one aluminium humidity chamber so that each sample could be positioned into the neutron beam without having to open the chamber. A second, smaller aluminium chamber contained a further D11 sample that had been prepared from a 100% D_2O suspension and dried under a D_2O atmosphere. The humidity inside the chambers was kept constant at 86% by the vapor of a saturated KCl solution kept in a small plastic vessel at the bottom of each chamber. The lamellar spacing under such conditions was 53.1 Å. For a rapid approach to the humidity equilibrium, an aquarium pump was installed which could blow the air from the chamber through a further KCl solution kept in a wash bottle outside

the chamber. A defined D_2O content of the hydrated samples was obtained by saturated KCl solutions of the desired D_2O/H_2O ratio.

The stability of the hydration and D_2O content was assayed by the variation of the lamellar spacing (≤ 0.2 Å) and of the intensities of the first and second lamellar reflections ($\leq 2\%$) over a period of 12 h. For a change in D_2O content of the samples, the saturated KCl solutions were adjusted to the new D_2O concentration and the atmosphere from the humidity cans was blown through the wash bottles for 24 h. Then pumping was stopped, and a final equilibrium as defined above was reached after a further 24 h.

Data Collection. The neutron diffraction experiments were carried out on the D16 diffractometer at the Institut Laue-Langevin, Grenoble, at a wavelength of 4.52 Å. The diffraction geometry was as described previously (Seiff et al., 1985; Mischel et al., 1987). Scans of the lamellar intensities were performed in two stages: a first, rapid $\theta-2\theta$ scan in sample and detector position for an overview of the diffraction pattern, and a second rocking curve scan with the detector positioned at the double Bragg angle (2θ) of the lamellar reflections (Mischel et al., 1987) for the collection of structural data. During the latter scan, only the sample was rotated in an interval of $\pm 1.5°$ at a step width of $0.1°$ around the corresponding Bragg angle (θ). A full set of data of the first to fifth lamellar reflections was usually collected by three scans of the latter type, each lasting over a period of about 4–7 h.

A 9° fwhm (full width at half-maximum) mosaic spread was obtained from a complete rocking curve ($\pm 10°$) of the fourth lamellar reflection of a D11 sample in a 100% D_2O atmosphere. In contrast to the rocking curves of lower order reflections, the latter is virtually unaffected by the increased extinction which occurs when the specimen is rotated so that either the main beam or the diffracted beam is parallel to the quartz slide substrate (Franks & Lieb, 1979). Neutron extinction was determined for all samples at every D_2O/H_2O ratio as well as for an empty stack of quartz slides.

Data Reduction. Data reduction was performed by integrating the intensities (corrected for inhomogeneities in the efficiencies of the detector cells) along 12 of the 16 vertical detector cells. Furthermore, data of the rocking curve scan were added together for sample positions around the optimal Bragg conditions (maximal intensity) when their variation of peak height was less than 1%. This resulted in taking the mean of the rocking curve around its maximum in an angular interval of ± 0.1, 0.4, 0.6, 0.8, and $1.2°$ for the $h = 1, 2, 3, 4$, and 5 reflections, respectively (h is the lamellar order number).

Determination of peak intensities was performed by fitting a Gaussian function to the data from which a linear or linear plus broad Gaussian background had been subtracted (see below). Corrected intensities $I_{cor}(h)$ were obtained from the observed intensities $I_{obs}(h)$ by

$$I_{cor}(h) = I_{obs}(h)\frac{h}{A(\theta)\ B(\theta)} \qquad (1)$$

where $A(\theta)$ is the extinction correction and $B(\theta)$ the acceptance correction due to the finite vertical aperture of the detector. The lamellar reflections are disklike in reciprocal space with a radius proportional to the order of reflection h. In a fixed $\theta-2\theta$ geometry, the Ewald sphere intersects these disks perpendicularly, thereby producing a sickle-like diffraction pattern in the detector. The part of the disk not cut by the Ewald sphere and extending into the third dimension in reciprocal space is not sampled in the detector. This is corrected by the Lorentz factor h. The extinction correction $A(\theta)$ was determined according to Franks and Lieb (1979), using the ex-
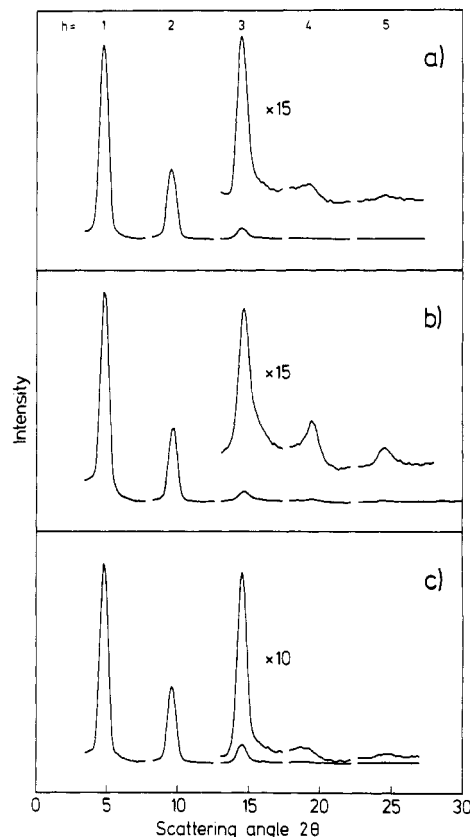

FIGURE 3: Uncorrected lamellar scattering intensities as determined from rocking curve scans (see text) at 0% relative D_2O and 86% relative humidity. (a) Pro-retinal BR. (b) Retinal-d_{11} BR. (c) Retinal-d_5 BR.

perimentally determined extinctions of $\mu l = 0.523, 0.514, 0.480,$ and 0.437 for 0, 10, 50, and 100% rel D_2O, respectively (μ is the linear extinction coefficient and l the thickness of the sample). The acceptance correction was calculated as the fraction of the reflected beam profile falling within the angular limits of the detector aperture. The profile of the reflected beam was determined as a convolution of the angular distribution of reflecting planes according to the mosaic spread (9°), the finite height of the sample (30 mm), and the divergence of the neutron beam (1°). For our specimens the acceptance correction was calculated as 0.903, 0.832, 0.758, 0.683, and 0.599 for the first to fifth order, respectively.

RESULTS

The lamellar neutron reflections could be recorded to a resolution of 10.6 Å for the three samples Pro-BR, D5-BR, and D11-BR at all relative D_2O concentrations applied (0, 10, 50, and 100% relative D_2O; due to limited machine time, data for 50 and 100% relative D_2O were only collected for the D11-BR sample). Figure 3 displays the uncorrected raw data for the three samples at 0% relative D_2O as determined from the rocking curve scans.

As visualized in the figure, the first-, second-, and fifth-order reflections sit on a fairly linear background which is probably caused by the isotropic scattering of the incoherent part of the proton/deuteron scattering cross sections and, in the case of the first order, is also due to some unblocked scattering of the zeroth order. For all reflections, the background is orders of magnitude larger than the scattering measured from an identical stack of empty quartz slides (not shown). Some additional broad and convex background underlies the third and fourth order. We ascribe this scattering to deviations from the mean structure of the PM stack, which do not exhibit
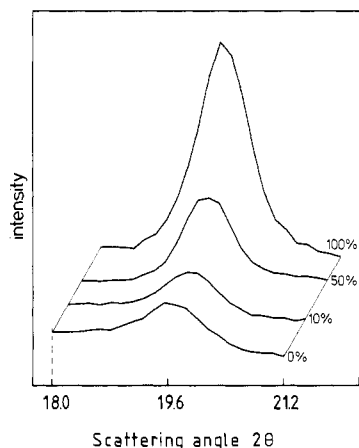
FIGURE 4: Dependence of the intensity of the fourth-order lamellar reflection for the D11-BR sample on the percentage D_2O.

long-range correlations (Cowley, 1975). Care was taken to separate this background from the Bragg peaks which represent the scattering by the mean unit cell (=mean over all unit cells that scatter coherently) (Cowley, 1975). All peaks were fitted by Gaussian functions with variable height, width, and center positions. In the case of the first, second, and fifth reflection a linear background was simultaneously fitted to the data points. As the fitted peak functions and the measured data points are virtually equal, no difference exists between the integrals calculated from fit parameters of the Gaussian fit and the integrals calculated directly by summing the data points after subtraction of the linear background for these reflections. For the third- and fourth-order reflection an additional broad Gaussian function was subtracted from the data in order to simulate the convex background underlying these peaks. This background Gaussian was chosen equal for all samples of equal D_2O/H_2O ratio. The position and width of the Gaussian function for the Bragg peak resulting after fitting the background-corrected data provided a cross check as to whether the background function had been chosen in a reasonable way. Both position and width of the third and fourth order fitted Bragg peaks, derived in this way, agree very well with expected values for these peaks according to the positions and widths of the first, second, and fifth order. An error for each peak intensity was estimated by repeating the fit procedure for several, extreme background functions chosen to obtain an obvious over- and underestimate of the Bragg intensities. The standard deviation σ was estimated as the largest of the absolute values of the differences between these upper and lower bounds and the best fit value. It should be noted that by taking only a linear background for the third and fourth order, their fitted intensities are well within the chosen 1σ width. We chose to present in Figure 3 the data at 0% D_2O at which the intensities are smallest. This creates an unfavorable impression of the background problem. With increasing percentage D_2O the intensities rise and uncertainties due to the background become less significant. Figure 4 is an expanded view of the data for the fourth-order reflection of the D11-BR sample at various percentages D_2O which shows that only at 0% D_2O a step in the background occurs and which gives a better impression of the quality of the data.

Tables I–III list the intensities corrected according to eq 1 for all the measured reflections at all D_2O/H_2O ratios. Tables I–III also contain estimated errors $[\sigma(h)]$ for the intensities derived from the counting statistics and from the uncertainty in the shape of the background as described above. Except for very weak intensities of some fourth- and fifth-order

Table I: Intensities $I_{cor}(h)$ Corrected According to Equation 1, Estimated Errors $\sigma(h)$, Errors Due to Counting Statistics $\sigma(h)_{count}$, and Fitted Intensities $I_{cal}(h)$ According to Equation 3 for the Lamellar Reflections in the H_2O–D_2O Exchange Experiment for the Retinal-d_{11} Sample[a]

h	1	2	3	4	5
$x = 0$					
$I_{cor}(h)$	2.74×10^4	1.14×10^4	1.34×10^3	499	424
$\sigma(h)_{count}$	82	46	13	15	17
$\sigma(h)$	1.40×10^3	550	455	72	42
$I_{cal}(h)$	2.97×10^4	1.20×10^4	1.46×10^3	476	390
$x = 0.1$					
$I_{cor}(h)$	1.15×10^5	4.02×10^3	1.24×10^3	492	289
$\sigma(h)_{count}$	130	80	33	17	20
$I_{cor}(h)^b$	1.18×10^5	3.95×10^3	1.74×10^3	482	200
$\sigma(h)_{count}{}^b$	140	40	23	18	24
$\sigma(h)$	6.00×10^3	300	480	63	55
$I_{cal}(h)$	1.06×10^5	3.87×10^3	1.37×10^3	503	291
$x = 0.5$					
$I_{cor}(h)^b$	9.09×10^5	3.31×10^4	2.22×10^3	985	93
$\sigma(h)_{count}$	1800	165	15	22	21
$\sigma(h)$	1.80×10^4	1.60×10^3	347	62	45
$I_{cal}(h)$	8.87×10^5	3.54×10^4	2.26×10^3	976	69
$x = 1.0$					
$I_{cor}(h)^b$	2.83×10^6	2.48×10^5	6.25×10^3	2.35×10^3	55
$\sigma(h)_{count}$	2800	250	63	35	14
$\sigma(h)$	5.70×10^4	1.20×10^4	364	300	25
$I_{cal}(h)$	2.93×10^6	2.19×10^5	6.24×10^3	2.39×10^3	52
$|F_{D11-BR,waterfit}|$	172	109	38.3	21.8	19.7
$|F_{W,waterfit}|$	1.54×10^3	565	79.8	42.7	27.0
$|(\phi_{D11-BR} - \phi_W)_{waterfit}|$	0	2.72	1.83	1.52	π
$\phi_{D11-BR,waterfit}$	π	± 2.72	± 1.31	± 1.52	0
$\phi_{D11-BR,labelfit}$	π	2.72	1.31	1.52	0

[a] x is the relative D_2O content of the sample. The absolute values for the structure factors of the retinal-d_{11} BR structure including H_2O and of the $(\rho_{D_2O} - \rho_{H_2O})$ structure as well as for the difference in phase angles $|\phi_P - \phi_W|$ according to the best fits in Table IV are given as $|F_{D11-BR,waterfit}|$, $|F_{W,waterfit}|$, and $|(\phi_{D11-BR} - \phi_W)_{waterfit}|$, respectively. $\phi_{D11-BR,labelfit}$ gives the phase for the retinal-d_{11} BR structure including H_2O according to the best fits for the retinal-d_{11} and -d_5 labels indicated in Tables V and VI (phase choice 1). [b] Second sample: retinal-d_{11} in small humidity chamber.

Table II: Intensities $I_{cor}(h)$ Corrected According to Equation 1, Estimated Errors $\sigma(h)$ for the Lamellar Reflections of the Pro-retinal BR sample, and Errors Due to Counting Statistics $\sigma(h)_{count}$[a]

h	1	2	3	4	5
$x = 0$					
$I_{cor}(h)$	2.78×10^4	1.11×10^4	2.04×10^3	200	88
$\sigma(h)_{count}$	83	33	20	15	20
$\sigma(h)$	1.39×10^3	550	200	40	44
$I_{cal}(h)$	3.00×10^4	1.05×10^4	2.13×10^3	145	74
$x = 0.1$					
$I_{cor}(h)$	1.10×10^5	3.66×10^3	1.85×10^3	86	25
$\sigma(h)_{count}$	110	37	19	12	10
$\sigma(h)$	5.00×10^3	180	185	40	15
$I_{cal}(h)$	1.05×10^5	3.64×10^3	1.90×10^3	144	35
$|F_{Pro-BR,labelfit}|$	176	104	46.9	12.3	8.72
$\phi_{Pro-BR,labelfit}$	-3.09	-2.63	1.16	-1.76	0.01
$|F_{D11,labelfit}|$	10.3	10.7	10.7	10.3	11.0
$\phi_{D11,labelfit}$	1.23	2.54	-2.56	-1.24	-0.01

[a] The calculated intensities $I_{cal}(h)$ are derived for the best fit (Table V) where a label according to eq 6 is subtracted from the retinal-d_{11} BR structure (phase choice 1). According to this phase choice, $|F_{Pro-BR,labelfit}|$, $\phi_{Pro-BR,labelfit}$, $|F_{D11,labelfit}|$, and $\phi_{D11,labelfit}$ give fitted structure factors and phases for the Pro-retinal BR structure including H_2O and for the retinal-d_{11} label alone. x is the relative D_2O content of the sample.

reflections, errors due to the latter cause are significantly larger than the errors caused by the counting statistics of peak and background [also given in Tables I–III by $\sigma(h)_{count}$] which are $\leq 1\%$ for the first to third order, $<14\%$ for the fourth, and $<20\%$ for most of the fifth-order reflections.

H_2O–D_2O *Exchange Experiments.* (*1*) *Determination of the D11-BR Phases, ϕ_P, Relative to the Water Phases, ϕ_W.* In order to solve the phase problem for a multilayer stack of

Table III: Intensities $I_{cor}(h)$ Corrected According to Equation 1, Estimated Errors $\sigma(h)$ for the Lamellar Reflections of the Retinal-d_5 BR Sample, and Errors Due to Counting Statistics $\sigma(h)_{count}$[a]

h	1	2	3	4	5
$x = 0$					
$I_{cor}(h)$	2.66×10^4	1.15×10^4	3.04×10^3	163	150
$\sigma(h)_{count}$	80	35	21	13	18
$\sigma(h)$	1.33×10^3	575	300	140	65
$I_{cal}(h)$	3.09×10^5	1.02×10^4	3.26×10^3	50	64
$x = 0.1$					
$I_{cor}(h)$	1.17×10^5	3.51×10^3	2.95×10^3	0	31
$\sigma(h)_{count}$	234	35	30	3	7
$\sigma(h)$	5.85×10^3	180	300	10	15
$I_{cal}(h)$	1.13×10^5	3.14×10^3	2.93×10^3	24	48
$\|F_{D5\text{-}BR,labelfit}\|$	169	97.0	54.6	6.05	7.21
$\phi_{D5\text{-}BR,labelfit}$	−3.10	−2.66	1.18	−2.32	1.02
$\|F_{D5,labelfit}\|$	7.82	7.82	7.82	7.82	7.82
$\phi_{D5,labelfit}$	0.452	0.904	1.35	1.80	2.26

[a] The calculated intensities $I_{cal}(h)$ are derived for the best fit (Table VI) where a label according to eq 6 is added to the calculated (Table II) Pro-retinal BR structure (phase choice 1). According to this phase choice, $\|F_{D5\text{-}BR,labelfit}\|$, $\phi_{D5\text{-}BR,labelfit}$, $\|F_{D5,labelfit}\|$, and $\phi_{D5,labelfit}$ give fitted structure factors and phases for the retinal-d_5 BR structure including H_2O and for the retinal-d_5 label alone. x is the relative D_2O content.
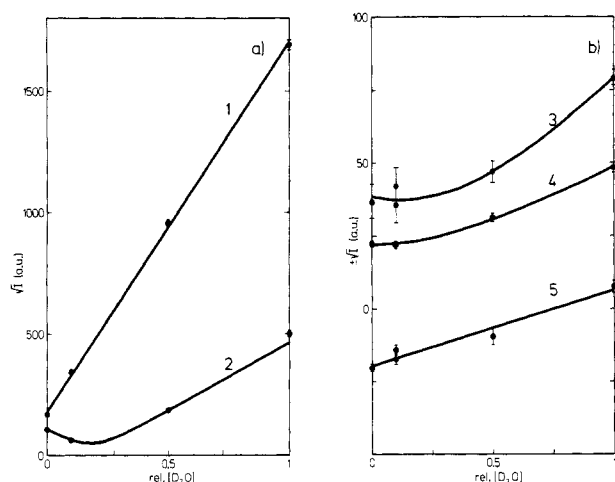

FIGURE 5: H_2O–D_2O exchange experiment for the retinal-d_{11} BR sample. $\sqrt{I}$ is the square root of the corrected intensity $I_{cor}(h)$ according to Table I. Error bars depict the estimated errors $\sigma(h)$, if the error exceeds the size of the data points. The data points are connected by lines corresponding to the best fit according to eq 3 and Table II. At 10% relative D_2O, there are two data points for every reflection. For $h = 1, 2$, and 4, these data points are the same within experimental error. (a) First and second lamellar reflection. (b) Third to fifth lamellar reflection. For convenience of display, the data of the fifth reflection for 0%, 10%, and 50% relative D_2O have been drawn as $-\sqrt{I}$.

purple membranes, a complete H_2O–D_2O exchange experiment was performed for the D11-BR sample (Figure 5). Limited machine time did not allow such experiments for all samples. The D11-BR sample was chosen for such an exchange experiment, because of its more intense fourth- and fifth-order reflections as compared to the Pro- and D5-BR samples (Figure 3). Actually, the exchange was performed in the small humidity chamber from 100% via 50% to 10% relative D_2O and in the big humidity chamber containing also the Pro- and D5-BR samples from 0% to 10% relative D_2O. At 10% D_2O there are two data points for every order in Figure 5 and Table I, one from each humidity chamber. For the $h = 1, 2$, and 4 reflections, the σ intervals of both data points overlap very well. For the $h = 3$ and 5 reflections the errors are larger, but the σ intervals of both intensity data points still overlap. Since oriented purple membrane films in the two chambers were prepared from the same batch of D11-BR and

since great care was taken to prepare the films in the same way, there is no a priori reason that a scaling factor should be applied between the data from both chambers. From Table I we note that scaling factors for the individual reflections would be (from $h = 1$ to $h = 5$): 1.026, 0.982, 1.403, 0.979, and 0.692. Since these numbers appear to be randomly distributed around the average of 1.016, there is no justification for a scaling factor that differs significantly from 1. The good agreement of the two unscaled data sets at 10% relative D_2O derived from the two independent samples (Table I and Figure 5) is an indication of the reproducibility of the relative D_2O content, the relative humidity, and the lamellar spacing, as well as of the sample preparation in general.

Initially, it had been assumed that the PM patches would stack onto each other in a random sidedness orientation on the quartz slide, so that the mean orientation within a domain (e.g., a ministack of PM patches), from which coherent scattering occurs, would be 50% up and 50% down (Worcester, 1975). In such a situation, the mean structure of the domain, calculated as the average over all repeating units, is centrosymmetric. For an idealized stack with no variation of unit cell length (no lattice disorder), but only random sidedness in each unit cell (substitutional disorder), the intensities seen in the Bragg reflections would then arise from scattering by the mean structure (i.e., centrosymmetric), whereas variations from the mean structure with no long-range order would be seen in the continuous diffraction underlying the Bragg peaks (Cowley, 1975). In a H_2O–D_2O exchange experiment, the scattering length at each point of the sample is a linear function of the isotopic composition of the water. Therefore, the Fourier transform (even if nonreal) of the scattering length density is expected to be a linear function of the relative D_2O content, $x = [D_2O]/([H_2O] + [D_2O])$, of the sample:

$$F(h) = F_P(h) + F_W(h)x$$
$$= |F_P(h)|e^{i\phi_P} + |F_W(h)|e^{i\phi_W}x \quad (2)$$

The expected intensity, $I_{cal}(h)$, is thus a quadratic function of x:

$$I_{cal}(h) = |F(h)|^2$$
$$= |F_P(h)|^2 + |F_W(h)|^2x^2 +$$
$$2 \cos(\phi_P - \phi_W)|F_P(h)||F_W(h)|x \quad (3)$$

In eqs 2 and 3 F_P represents the structure factor of the complete unit cell containing the protein, lipids, and H_2O; F_W is the Fourier coefficient of the difference scattering density due to the replacement of H_2O by D_2O accounting for the H_2O–D_2O exchange; and ϕ_P and ϕ_W are the corresponding phases. In the centrosymmetric case the structure factors are real, i.e., a fortiori $\cos(\phi_P - \phi_W) = \pm 1$, and therefore, even the absolute values of the structure factors $|F(h)|$ will be a linear function of the D_2O concentration (Bragg & Perutz, 1952; Perutz, 1954; Franks & Lieb, 1979).

Figure 5 shows that for the first and fifth order, the absolute values of the structure factors are good linear functions of the D_2O/H_2O ratio. For the second-order structure factors the absolute values may at first sight also be approximated by a straight line, when the points at 50% and 100% D_2O are reflected in the horizontal axis (i.e., a phase change around $x = 0.2$). For $h = 2$ as well as for $h = 3$ and 4 the straight-line fit was rejected, however, by the following quantitative analysis of the deviations from linearity.

For this purpose, the experimentally determined intensities, weighted by the estimated errors (Table I), were fitted to a parabolic function according to eq 3 [Marquardt procedure (Bevington, 1969)]. Alternatively, the value of $\cos(\phi_P - \phi_W)$ was kept constant at ± 1 (straight-line fit). The first fit pro-

Table IV: Results of Fitting Equation 3 to the Measured Intensities of the H_2O–D_2O Exchange Experiment for the Retinal-d_{11} BR Sample (Table I) in the Centrosymmetric and Noncentrosymmetric Cases

h	1	2	3	4	5
χ_{sym}^2 ($N_{free} = 3$)	4.31	10.0	2.04	1.40	1.61
$\|\phi_P - \phi_W\|$	0	π	0	0	π
$\|F_P\|$	172	116	29.5	20.2	19.7
$\|F_W\|$	1.54×10^3	593	48.0	25.8	27.0
χ_{asym}^2 ($N_{free} = 2$)	6.47	4.77	0.34	0.12	2.15
$\|\phi_P - \phi_W\|$	0.00	2.72	1.83	1.52	2.88
$\|F_P\|$	172	109	38.3	21.8	19.5
$\|F_W\|$	1.54×10^3	565	79.8	42.7	24.5
F_χ	-1.54×10^3	4.29	16.0	33.0	0.247
$P_F(F_\chi,1,N_{free,asym})$ (%)	>50	17	6	3	>50

vides the three parameters $\|F_P(h)\|$, $\|F_W(h)\|$, and $\|\phi_P - \phi_W\|$, whereas the latter straight-line fit gives $\|F_P(h)\|$, $\|F_W(h)\|$ and the discrete value for $\|\phi_P - \phi_W\|$ as 0 or π. Results of both fits are listed in Table IV, where χ^2 was evaluated as

$$\chi^2 = \frac{1}{N_{free}} \sum_i \frac{1}{\sigma_i^2}(I_{cal}^i - I_{cor}^i)^2 \qquad (4)$$

where N_{free} is the number of the degrees of freedom and σ the estimated error in intensity. The sum is taken over all intensities considered in the fit. According to the χ^2 criterion (Table IV), a straight-line fit is superior for $h = 1$ and 5, whereas the nonlinear fit is superior for $h = 2$, 3, and 4. However, one should not emphasize the absolute values of χ^2 too much, as they depend in a sensitive way on the estimates for the errors of the data. The significance of an additional parameter in the fit function, in our case values for $\|\phi_P - \phi_W\|$ different from 0 or π, can be estimated by the F_χ test (Bevington, 1969):

$$F_\chi = \frac{N_{free,sym}\chi_{sym}^2 - N_{free,asym}\chi_{asym}^2}{\chi_{asym}^2} \qquad (5)$$

From the F distribution the probability $P_F(F_\chi,1,N_{free,asym})$ can be calculated that the addition of a set of random numbers to the symmetrical (linear) fit function would improve the quality of the fit as much as the inclusion of an additional term (in this case the nonlinear term for $\|\phi_P - \phi_W\|$ different from 0 or π). Values for F_χ and $P_F(F_\chi,1,N_{free,asym})$ are also included in Table IV.

Probabilities of more than 50% to produce the same result by random numbers clearly suggest that the asymmetric fit for reflections 1 and 5 is inferior to the symmetric (straight-line) fit. It is therefore suggested that the structure factors of the protein and water for these lamellar reflections are collinear in the complex plane [cos ($\phi_P - \phi_W$) = ±1]. On the other hand, for reflections 2–4, the parabolic fits are significantly better, with probabilities of only 17%, 6%, and 3%, respectively, to produce the same quality of fit by addition of random numbers to the straight-line fit. This indicates that by at least 83% probability the structure factors of these reflections for the protein and the water are not collinear. The angle between their vectors is derived from the fit. For $h = 2$ the linear fit with $\phi_P - \phi_W = \pi$ (see Table IV) gives a very good fit for the unweighted data. If the data are properly weighted, however, the parabolic fit is clearly superior according to the $P_F(F_\chi,1,N_{free,asym})$ criterion. We note that for $h = 2$ the phase of 2.72 is already so close to π that no major change is expected in the label positions, if this phase is set equal to π. Further analysis supports this point. For orders 3 and 4, however, the phases are not close to either 0 or π. The improvement of the parabolic fit is particularly

pronounced for the $h = 4$ reflection [there is a $1 - P_F(F_\chi,1,N_{free,asym}) = 97\%$ probability that the improvement is not caused by chance], for which the errors are small, the overlap between the data from the two chambers at 10% D_2O is excellent, and the χ^2 for a straight line is 10 times larger than for a parabola. The absolute values for the structure factors of the retinal-d_{11} BR structure including H_2O ($\|F_P\|$) and of the ($\rho_{D_2O} - \rho_{H_2O}$) structure ($\|F_W\|$) as well as for the difference in phase angles $\|\phi_P - \phi_W\|$ according to the best fits in Table IV have been included in Table I as $\|F_{D11\text{-}BR,waterfit}\|$, $\|F_{W,waterfit}\|$, and $\|(\phi_{D11\text{-}BR} - \phi_W)_{waterfit}\|$, respectively. Table I also lists the calculated intensities $I_{cal}(h)$ according to eq 3.

If the stacks were centrosymmetric, then the plots in Figure 5 should be linear for *all* reflections. This is rejected by our analysis as summarized in Table IV. We therefore conclude that the scattering length density, the Fourier transform of which is sampled by the Bragg reflections, is not centrosymmetric, a situation that would arise when the single PM patches do not form domains (microstacks) of random sidedness orientation. Sidedness order could be caused by electrical or steric side-specific forces between PM patches (see Discussion). Direct evidence for the existence of such asymmetric stacks in PM films was recently obtained by the observation of optical second harmonic generation (Huang et al., 1989; Huang & Lewis, 1989). This effect is strictly forbidden in a centrosymmetric structure.

(2) Assignment of Water Phases, ϕ_W. As long as there is no further information about the water distribution, the phase problem for the retinal-d_{11} BR cannot be solved from the absolute values of phase angle differences $\|\phi_P - \phi_W\|$ given in Table IV. At this point the approximation was introduced that the water distribution at our resolution of 10.6 Å is essentially Gaussian and is centered between two membrane patches. This approximation arises partly from the fact that a completely dried purple membrane stack still exhibits a lamellar spacing of 48 Å (Henderson, 1975). The centrosymmetric layers of free water between the membranes would therefore have a thickness of 5 Å in our experiments. Furthermore, the lipid headgroups are separated by 40 Å (Blaurock, 1975). Water extending from the bulk toward the lipid headgroups would therefore partly occupy a further layer of 8 Å. Lack of centrosymmetry in the water distribution could be caused by lack of centrosymmetry of the protein in this remaining layer of 8 Å, which is slightly beyond the experimental resolution of 10.6 Å. Water extending further into the protein as a channel cannot be completely ruled out (Zaccai & Gilmore, 1979), but its relative contribution to the water content of the whole lamellar stack may be small. An additional justification for the assumed centrosymmetry of the water layer derives from the fact that it leads to a consistent interpretation of the two other isomorphous replacement experiments (retinal-d_{11} and -d_5) which were carried out simultaneously (see below). A Gaussian water profile with the origin of the lamellar axis halfway between two neighboring water layers, i.e., near the middle of the membrane, leads to an unambiguous assignment of the water phases, ϕ_W, as π, 0, π, 0, and π for the first to fifth lamellar water structure factors (Franks & Lieb, 1979).

On the basis of the result that ϕ_W is either π or 0, the fit results for $\|\phi_P - \phi_W\|$ (Table IV) can be translated into values for ϕ_P alone. The ambiguity for the sign of the difference ($\phi_P - \phi_W$) results in an ambiguity for the second- to fourth-order protein phases. These phases ϕ_P ($=\phi_{D11\text{-}BR}$) can be expressed as π, ±2.72, ±1.31, ±1.52, and 0 rad for the first to fifth order, respectively. These phases have been included into Table I as $\phi_{D11\text{-}BR,waterfit}$.

Table V: Results of Fitting the Density Distribution for the Retinal-d_{11} Label According to Equation 6 to the Measured Intensities for the Retinal-d_{11} and Protonated Retinal BR Samples at 0% and 10% Relative D_2O^a

phase choice	χ^2	A	α	d (Å)	b (Å)	S
1: + + + + +	1.568	27.6	0.000	10.5	1.69×10^{-3}	1.033
2: + + − + +	4.005	45.0	0.200	9.68	1.70×10^{-3}	1.030
3: + + − − +	6.587	24.2	0.949	10.6	1.18×10^{-3}	0.979
4: + + + − +	9.700	27.9	0.862	10.2	1.11×10^{-3}	0.949

^{a} A, α, d and b are the label strength, sidedness order parameter, label position, and label width (eq 6). The scaling factor S derived from the fit gives the ratio of the corrected intensities of the D11- to Pro-BR samples. Phase choices give the signs multiplying the absolute values of phases for the retinal-d_{11} BR structure ($|\phi_{D11-BR,waterfit}|$) according to Table I in the order of the first to fifth reflection.

Table VI: Results of Fitting the Density Distribution for the Retinal-d_5 Label According to Equation 6 to the Measured Intensities for the Retinal-d_5 and Protonated Retinal BR Samples at 0% and 10% D_2O^a

phase choice	χ^2	A	α	d (Å)	b (Å)	S
1: + + + + +	4.211	19.6	0.000	3.82	1.69×10^{-3}	1.088
2: + + − + +	21.88	16.8	0.010	4.70	3.50×10^{-3}	1.061
3: + + − − +	23.17	14.2	0.000	9.12	2.00×10^{-3}	1.005
4: + + + − +	15.64	122	0.318	−3.48	3.48	1.490

^{a} The scaling factor S derived from the fit gives the ratio of the corrected intensities of the Pro- to D5-BR samples.

The ambiguity in sign for the phase angles of the protein reflections 2–4 should result in 2^3 possibilities for the retinal-d_{11} BR structure. However, every two of them are related by a mirror axis in the middle of one unit cell, so that there will be four independent solutions to the phase problem. These four independent solutions have been labeled as phase choices 1–4 with the following signs for the phases $\phi_{D11-BR}(h)$: +++++, ++−++, ++−−+, and +++−+, for h = 1–5, respectively.

Location of the Ring (D11) and Schiff Base (D5) Labels. In order to simulate the scattering length density of the ring-labeled retinal within the multilayer stack of purple membranes, a model function of two Gaussians placed at symmetric positions ($\pm d$) with respect to the center of the membrane, with identical bandwidths (b), but with allowance for asymmetry in amplitudes $[(1 - \alpha)A, \alpha A]$ was introduced:

$$\rho_{label} = \frac{A}{\sqrt{\pi}b}\left\{(1 - \alpha) \exp\left[-\left(\frac{x - d}{b}\right)^2\right] + \alpha \exp\left[-\left(\frac{x + d}{b}\right)^2\right]\right\} \quad (6)$$

This function simulates the case of one asymmetric label per one unit cell, which is sampled in the Bragg reflections as an average over the whole domain from which coherent scattering occurs. Within this domain the single unit cells have a certain degree of sidedness orientation (complete orientation: $\alpha = 0$ or $\alpha = 1$; random orientation: $\alpha = 0.5$).

The Fourier transform of eq 6 was calculated and subtracted from the four possible sets of structure factors of the D11-labeled membranes according to Tables I–III ($|F_{D11-BR,waterfit}|$, $\phi_{D11-BR,waterfit}$) in order to derive simulated structure factors and scattering intensities for the unlabeled membrane. These modeled intensities were fitted to the observed intensities of the protonated (Pro) retinal BR sample at 0% and 10% D_2O by variation of the parameters in eq 6 and with the additional freedom of an overall scaling factor between the corrected D11 and Pro intensities given in Tables I–III. The fit was carried out for the four independent phase choices possible for the retinal-d_{11} membrane which result from the ambiguity in the sign of the phase differences in the $H_2O–D_2O$ exchange experiment (see above). In a completely analogous way, a model scattering length distribution of the retinal-d_5 label was assumed according to eq 6, added in reciprocal space to the structure factors of the protonated membrane obtained from the D11 label fit, and used to simulate the measured intensities of the BR sample labeled with retinal-d_5 at 0% and 10% relative D_2O content.

Results of both fits are listed in Tables V and VI for the four possible sets of phases. As is evident from Table V, there is one good fit of the retinal-d_{11} label (χ^2 = 1.568), corre-

sponding to phase choice 1 (signs of the phases ϕ_{D11-BR}: +++++), and a second fit with higher χ^2 (4.005) for phase choice 2 (phase signs: ++−++). Phase choices 3 (++−−+) and 4 (+++−+) seem very unlikely according to the χ^2 distribution. For the retinal-d_5 label fit (Table VI) phase choise 1 also yields the best χ^2. The second best fit (phase choice 4) is highly unlikely due to the large scaling factor S (1.490) and the too large label strength A as compared to the retinal-d_{11}. For the retinal-d_5 the absolute values of χ^2 are higher than for the retinal-d_{11}. This can be the result either of an underestimation of the errors in intensities or of error propagation; the phases of the protonated membrane which are essential input data to the fit have been derived via the $H_2O–D_2O$ exchange in the D11 sample and the subtraction of the fitted D11 label. In any case, for both labels, phase choice 1 results in the best χ^2, and already phase choice 2 (second best fit for D11 and third best fit for D5) is significantly less likely as judged by their χ^2. For all phase choices (except the unreasonable phase choice 4), the label strength A of the retinal-d_{11} exceeds the label strength of the retinal-d_5 by a factor of 1.4–2.7, whereas a factor of 2.2 would be expected from the number of deuterons. For the two best phase choices the sidedness order parameter α of the label distribution is less than 0.2 for the D11 and D5 labels. Thus for these two independently prepared samples α is close to zero, indicating that the domain, from which coherent scattering occurs, exhibits almost perfect sidedness orientation. The very small widths b of the label, on the order of 10^{-3} Å for all cases (except phase choice 4, retinal-d_5), only indicate that the label widths are well below the experimental resolution. In fact, a label function modeled as a δ distribution could have produced the same results, thereby reducing the number of fit parameters by one. For all phase choices (except 4, retinal-d_5), the scaling factor S is close to 1 ($\pm 9\%$). This would be expected for the identical preparations of the different samples.

For the best phase choice (1, signs of the phases ϕ_{D11-BR}: +++++) we have included the absolute values of protein structure factors as $|F_{Pro-BR,labelfit}|$, $|F_{D5-BR,labelfit}|$, $|F_{D11,labelfit}|$, and $|F_{D5,labelfit}|$ in Tables II and III; the corresponding phases for the proteins and labels have also been included in Tables I–III as $\phi_{Pro-BR,labelfit}$, $\phi_{D5-BR,labelfit}$, $\phi_{D11,labelfit}$, $\phi_{D5,labelfit}$.

The scattering length distributions for the protonated retinal and retinal-d_{11} and -d_5 labeled membranes, as well as for the labels alone, have been calculated as the Fourier transforms of the fitted structure amplitudes and phases. They are depicted in Figure 6 according to phase choice 1 (values of the phases are given in the figure legend). The scattering length distributions of the two labels according to phase choice 2 are quite similar (see also Tables V and VI). In either case, the retinal-d_5 label is located near the center of the membrane, whereas the retinal-d_{11} label is positioned at a distance of about 5.0–6.8 Å from the D5 label toward the membrane side with higher scattering density. As the unweighted R factors ($\sum ||F_{cor}| - |F_{cal}||/\sum|F_{cor}|$) are small for the D11 label (3.2%)
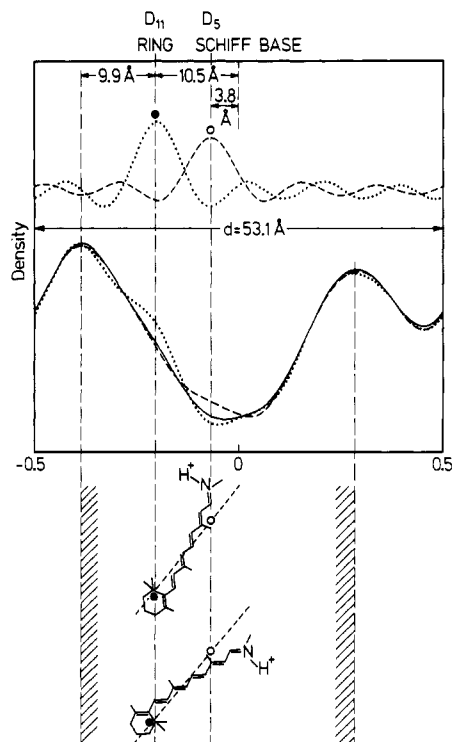
FIGURE 6: Projected scattering length density along the lamellar z axis. The position along this axis is expressed in units of the lamellar repeat distance of 53.1 Å. Middle panel: Density of the purple membrane with and without labels [(—) Pro-retinal BR; (⋯) retinal-d_{11} BR; (- - -) retinal-d_5 BR]. Upper panel: Calculated densities of the labels alone [(⋯) retinal-d_{11}; (- - -) retinal-d_5] scaled by a factor of 3. Lower panel: The two possible orientations of the plane of the chromophore. The line joining the centers of deuteration of the two labels (- - -) makes an angle of 40° with the plane of the membrane. Only the top choice is in agreement with the known orientation of the polyene chain of approximately 20° (Heyn et al., 1977). Densities were calculated according to phase choice 1: $\phi_{D11\text{-}BR}(h) = \pi$, 2.72, 1.31, 1.52, 0; $\phi_{Pro\text{-}BR}(h) = -3.09, -2.63, 1.16, -1.76, 0.01$; $\phi_{D5\text{-}BR}(h) = -3.10, -2.66, 1.18, -2.32, 1.02$.

and the D5 label (5.7%) for phase choice 1, there is virtually no difference in scattering length distributions if they are derived either from measured or from calculated structure factor amplitudes.

The same label positions are also derived from a Fourier difference map (not shown) with all phases set to the values of phase choice 1 of the retinal-d_{11} BR sample (Table V). In this case, the labels are not so well shaped because of errors inherent to the difference Fourier method which become more pronounced if the number of reflections is small.

DISCUSSION

The present investigation establishes the positions of the cyclohexene ring (D11) and the Schiff base end (D5) of the chromophore of BR with respect to the one-dimensional projection of the neutron scattering density of the PM onto a line perpendicular to the membrane plane. The experimental setup consisted of multilamellar stacks of dried purple membranes at 86% relative humidity, exhibiting a defined lamellar spacing of 53.1 Å with Bragg peaks up to the fifth order. This is in contrast to previous neutron diffraction studies on the transmembrane position of perdeuterated retinal (King et al., 1979) in which the continuous diffraction of a suspension of PM sheets was measured and direct methods for the solution of the phase problem were used.

Our approach to the phase problem was the isomorphous replacement of H_2O by D_2O in a sample of PM labeled with

retinal-d_{11}. This experiment leads to the conclusion that the lamellar stacking of PM patches induced by slow drying of PM suspensions in deionized water leads to the formation of coherent domains where siddedness order of PM patches exists. The results of the isomorphous H_2O–D_2O exchange allow four independent phase choices for the PM labeled by retinal-d_{11}. In a second isomorphous replacement, retinal-d_{11} was exchanged to perprotonated retinal (Pro) and from the best fit in reciprocal space by a model label function (eq 6), the best (1) of the four phase choices, the position of the label, and the phases of the PM with Pro-retinal have been obtained. In an analogous way, the position of the D5 label, the phases of PM labeled by retinal-d_5, and an independent best phase choice have been determined in a further replacement of Pro-retinal by retinal-d_5. This independent best phase choice (1) coincides with the previous best phase choice for the retinal-d_{11} PM.

The conclusion of the H_2O–D_2O exchange experiment that the PM patches orient on the quartz slide as domains of definite siddedness, i.e., as asymmetric stacks, may be surprising at first sight but seems rather plausible when the large charge difference of the two BR membrane surfaces is considered. This difference was determined as more than 0.007 e/Å^2 (Renthal & Cha, 1984), giving rise to an effective (screened in part by counterions) permanent dipole moment per BR molecule of 98 D (Kimura et al., 1984) or even 10^3 D (Keszthelyi, 1980) directed from the cytoplasmic to the extracellular side. PM in suspensions therefore orients easily even in low electric fields of the order of 20 V/cm. If two BR monomers (transmembrane length 48 Å) are stacked at a distance of 5 Å on top of each other, one could estimate the difference in electrostatic interaction energy for the two relative orientations up–up and up–down. A 98-D permanent dipole could arise from a net charge difference of 0.4 elementary charges at a distance of 48 Å (i.e., the membrane thickness). For this case (point charges), the energy difference for both orientations is 0.006 eV ($\epsilon = 81$). Even in the dipole–dipole interaction approximation, this energy difference amounts to 0.002 eV (98 D, $\epsilon = 81$). For the situation of two adjacent PM patches, electrostatic interactions between all monomers have to be added. The energy difference for the monomer orientations is at least multiplied by the number of BR monomers in one patch, if only next-neighbor interactions are taken into account. As even a small patch of 200-nm diameter contains about 3000 BR molecules, the energy difference is of the order of 10 eV. Even if the BR charges are further screened to some extent by their counterions, it is hard to imagine how the energy difference for both orientations can drop below the thermal energy of 0.025 eV. Therefore, in thermal equilibrium two PM patches would stack onto each other in an aligned orientation. The question arises whether this equilibrium can be reached. As the samples are prepared from rather "dilute" ($\approx$1 mM BR) PM suspensions, some freedom of rotation for single patches exists at the beginning of the drying process. One patch may orient in the electric fields of its neighbors. As the drying proceeds, complete rotations of a patch will be suppressed by the increasing density of surrounding patches. However, even at this higher density, a sidedness oriented stack of PM patches might still form from a random sidedness stack by squeezing out all PM patches of one orientation laterally toward neighboring stacks of the corresponding orientation. In this way, a slow drying process of several days might permit the formation of well-aligned microdomains which could be surrounded by oriented domains of the opposite alignment. Recently, optical second harmonic generation was observed from the chromophore of BR in a

stack of purple membranes (Huang et al., 1989). Since this nonlinear optical effect is strictly forbidden in a centrosymmetric structure on symmetry grounds, its observation is direct evidence for the existence of asymmetric stacks. Our conclusion that the absolute values of the structure factors in the contrast variation experiment fall on nonlinear curves (Figure 5) is supported by the only other work on lamellar neutron diffraction of purple membranes (Worcester, 1975). At that time only the first two orders could be observed. High-quality data at five different D_2O/H_2O ratios led to a perfect straight line for $h = 1$, whereas a clear deviation from linearity was observed for $h = 2$.

Absolute positions of the label center, d, given in Tables V and VI are with respect to an origin halfway between two intermembrane, centrosymmetric water layers. This origin therefore represents only approximately the center of the PM defined by its scattering length distribution (Figure 6). Two fixed points within the PM scattering density may be defined by the maxima of scattering density (Figure 6) near both membrane surfaces. These maxima are presumably due to an abundance of amino acids with low proton content near the surface (e.g., Phe, Tyr, Trp) predicted by various amino acid sequence folding models [e.g., Huang et al. (1982)], and/or by the glycerol phosphate and sugar-containing headgroups of the lipids, which also contain only few protons. The distance between these two maxima is 35 Å (Figure 6, middle panel). A similar profile was obtained in the work of King (King et al., 1979), although the resolution was rather limited (≤ 0.07 Å^{-1}). It should be noted that the scattering density projection onto the lamellar axis for X-rays and electrons may differ substantially from the neutron scattering length distribution, because hydrophilic and hydrophobic amino acids vary considerably in their relative cross sections for the respective radiations. Furthermore, the main contributions of the lipids to the X-ray and electron scattering arise from the phosphates, whereas for neutrons scattering density maxima are expected for the sugar residues with low hydrogen content. In the two-dimensional projection onto the membrane plane, these differences may cancel, as the scattering densities are averaged along the membrane normal, but for a one-dimensional projection onto the membrane normal, these differences will not cancel, because hydrophobic and hydrophilic membrane slices are averaged separately.

With respect to the left density maximum, as a fixed point near the membrane surface, the cyclohexene ring (D11) is positioned at a depth of 9.9 Å and the Schiff base label (D5) at 16.6 Å for phase choice 1 (Figure 6, top panel). For phase choice 2 the corresponding numbers are 7.6 and 12.6 Å. By use of the intensity errors and computer simulation, the errors in the label positions are estimated to be ±1.2 Å for the D11 label and ±1.5 Å for the D5 label. From the distance of 6.7 Å between the projected label positions (phase choice 1) and the distance of 10.6 Å between the centers of mass of the two labels in the structure of *all-trans*-retinal in BR (Harbison et al., 1985), a value of 40° is obtained for the angle between the vector connecting the label positions and the plane of the membrane. Since the line between the D5 and D11 centers of mass makes an angle of 15° with the all-trans polyene chain and since the plane of the chromophore is approximately perpendicular to the plane of the membrane (Earnest et al., 1986; Ikiegami et al., 1987; Heyn et al., 1988), the tilt angle which the polyene chain makes with the plane of the membrane is 40 ± 15°. Of these two possibilities shown in the bottom panel of Figure 6, only the 25° solution is compatible with the known tilt angle of the polyene chain which has values

between 20 and 25° (Heyn et al., 1977; Bogomolni et al., 1977; Bamberg et al., 1979). In this geometry (bottom panel of Figure 6, top) the N→H bond of the Schiff base points toward the same membrane surface as the vector from the Schiff base to the cyclohexene ring. In the alternative geometry, which we can reject, the chromophore is rotated around the interlabel axis by π, the N→H and N→C$_5$ vectors point to opposite membrane surfaces, and the tilt angle of the chain is 55° (bottom panel of Figure 6, bottom). If we consider the errors in the label positions discussed above, the two possible tilt angles of the polyene chain are 55 ± 12° and 25 ± 12° and it is still possible to conclude that the N→H bond and N→C$_5$ vector should point toward the same side of the membrane. The same conclusion was recently obtained on the basis of linear dichroism experiments with 3,4-dehydroretinal (Lin & Mathies, 1989). Since the chromophore is most likely closest to the extracellular surface (see discussion below), this result means that the N→H bond of the Schiff base points toward that surface and puts constraints on the possible residues with which the Schiff base proton may interact in the ground state. A direct interaction with Asp-212 would be possible [see also Lin and Mathies (1989)]. It can be shown that a 13-cis isomerization of the dark-adapted retinal would change the predicted angles by no more than 4° and would not affect the argument. The same conclusions are reached with phase choice 2. However, error propagation in the protonated and retinal-d_5 PM phases as well as the lower label strength of retinal-d_5 render the retinal-d_5 label position certainly less well-defined than the D11 position (computer-simulated error estimates are 1.5 and 1.2 Å, respectively). Further work on an independent determination of protonated and retinal-d_5 phases would be desirable.

The depth of the retinal in BR along the transmembrane axis has been determined before by fluorescence energy transfer experiments with the chromophore as either donor or acceptor (Tsetlin et al., 1983; Kouyama et al., 1988a; Otomo et al., 1988; Leder & Thomas, 1986; Leder et al., 1989), by resonance Raman (Nabiev et al., 1985), and by continuous neutron diffraction on PM suspensions (King et al., 1979). All optical experiments place the center of the transition dipole of retinal at a distance of 6–13 Å from the point of closest approach to the membrane surface for an external energy transfer donor or acceptor. Continuous neutron diffraction experiments, on the other hand, located the perdeuterated retinal at the center of the membrane (King et al., 1979). The present study resolves this discrepancy to some extent, as the retinal cyclohexene ring is unambiguously positioned off the center (Figure 6); however, the Schiff base end of the retinal still resides close to the center, but slightly shifted toward the same membrane side as the ring (Figure 6).

Disagreement persists in the results of optical experiments whether the center of the retinal transition dipole should reside within the extracellular (Nabiev et al., 1985; Leder et al., 1989) or the cytoplasmic (Otomo et al., 1988; Tsetlin et al., 1983) half of the membrane. Photoaffinity labeling experiments place the cyclohexene ring in the neighborhood of amino acids Ser-193 and Glu-194 (Huang et al., 1982), which are predicted to be close to the extracellular surface in current folding models of BR. Assuming that the Schiff base proton is directly involved in the charge translocation and that the protein is homogeneous with respect to the dielectric constant, time-resolved photoelectric experiments place the Schiff base closer to the extracellular membrane side (Keszthelyi & Ormos, 1980; Holz et al., 1988). From the present investigation alone, the side of the membrane to which the chromophore is closest

cannot be determined, as too little is known about the cause for the asymmetric neutron scattering length density of the PM (Figure 6), which could be the protein itself and/or the asymmetric lipid distribution (Renthal & Cha, 1984). The most recent energy transfer experiments with envelope vesicles (Leder et al., 1989) conclude that the transition dipole is 10 ± 2 Å from the extracellular membrane surface. When we localize the transition dipole in the middle of the polyene chain, this distance is in reasonable agreement with the present result. By use of an optical second-harmonic interference technique it was recently shown that the vector from the Schiff base to the cyclohexene ring points toward the extracellular surface (Huang & Lewis, 1989). Together with our results, this means that the chromophore is closer to the extracellular side and that the left-hand membrane surface in Figure 6 is the extracellular surface. Further experiments with side-specific surface labels should provide a definitive answer.

In conclusion, we have determined the depths of the label positions in the cyclohexene ring and near the Schiff base separately using partially deuterated retinals. The vector from the Schiff base to the ring points toward the nearest membrane surface, most likely the extracellular surface. This vector connecting the two label positions in the chromophore makes an angle of 40 ± 12° with the plane of the membrane. These results are summarized in Figure 6 (top part of bottom panel).

REFERENCES

Baldwin, J. M., Henderson, R., Beckmann, E., & Zemlin, F. (1988) *J. Mol. Biol. 202*, 585–591.

Bamberg, E., Apell, H. J., Dencher, N. A., Sperling, W., Stieve, H., & Läuger, P. (1979) *Biophys. Struct. Mech. 5*, 277–292.

Bevington, P. R. (1969) *Data Reduction and Error Analysis for the Physical Sciences*, McGraw-Hill Book Co., New York.

Blaurock, A. E. (1975) *J. Mol. Biol. 93*, 139–158.

Bogomolni, R. A., Hwang, S. B., Tseng, Y. W., King, G. I., & Stoeckenius, W. (1977) *Biophys. J. 17*, 89a.

Bragg, W. L., & Perutz, M. F. (1952) *Acta Crystallogr. 5*, 277–283.

Braun, D., Dencher, N. A., Fahr, A., Lindau, M., & Heyn, M. P. (1988) *Biophys. J. 53*, 617–621.

Cowley, J. M. (1975) *Diffraction Physics*, North-Holland Publishing Co., Amsterdam.

Drachev, L. A., Kaulen, A. D., & Skulachev, V. P. (1984) *FEBS Lett. 178*, 331–335.

Earnest, T. N., Roepe, P., Braiman, M. S., Gillespie, J., & Rothschild, K. J. (1986) *Biochemistry 25*, 7793–7798.

Franks, N. P., & Lieb, W. R. (1979) *J. Mol. Biol. 133*, 469–500.

Grzesiek, S., & Dencher, N. A. (1986) *FEBS Lett. 208*, 337–342.

Harbison, G. S., Smith, S. O., Pardoen, J. A., Courtin, J. M. L., Lugtenburg, J., Herzfeld, J., Mathies, R. A., & Griffin, R. G. (1985) *Biochemistry 24*, 6955–6962.

Hauss, T., Otto, H., Grzesiek, S., Westerhausen, J., & Heyn, M. P. (1989) *Biophys. J. 55*, 254a.

Henderson, R. (1975) *J. Mol. Biol. 93*, 123–138.

Heyn, M. P., Cherry, R. J., & Müller, U. (1977) *J. Mol. Biol. 117*, 607–620.

Heyn, M. P., Westerhausen, J., Wallat, I., & Seiff, F. (1988) *Proc. Natl. Acad. Sci. U.S.A. 85*, 2146–2150.

Holz, M., Lindau, M., & Heyn, M. P. (1988) *Biophys. J. 53*, 623–633.

Huang, J. Y., & Lewis, A. (1989) *Biophys. J. 55*, 835–842.

Huang, J. Y., Chen, Z., & Lewis, A. (1989) *J. Phys. Chem. 93*, 3314–3320.

Huang, K. S., Radhakrishnan, R., Bayley, H., & Khorana, H. G. (1982) *J. Biol. Chem. 257*, 13616–13623.

Ikegami, A., Kouyama, T., Otomo, J., Urabe, H., Fukuda, K., & Kataoka, R. (1987) in *Retinal Proteins* (Ovchinnikov, Y., Ed.) pp 37–45, VNU Science Press, Utrecht, The Netherlands.

Keszthelyi, L. (1980) *Biochim. Biophys. Acta 598*, 429–436.

Keszthelyi, L., & Ormos, P. (1980) *FEBS Lett. 109*, 189–193.

Kimura, Y., Fujiwara, M., & Ikegami, A. (1984) *Biophys. J. 45*, 615–625.

King, G. I., Stoeckenius, W., Crespi, H. L., & Schoenborn, B. P. (1979) *J. Mol. Biol. 130*, 395–404.

Kouyama, T., Kinoshita, K., Jr., & Ikegami, A. (1988a) *Adv. Biophys. 24*, 123–175.

Kouyama, T., Nasuda-Kouyama, A., Ikegami, A., Mathew, M. K., & Stoeckenius, W. (1988b) *Biochemistry 27*, 5855–5863.

Leder, R. O., & Thomas, D. D. (1986) *Biophys. J. 49*, 212a.

Leder, R. O., Helgerson, S. L., & Thomas, D. D. (1989) *J. Mol. Biol. 209*, 683–701.

Lin, S. W., & Mathies, R. A. (1989) *Biophys. J. 56*, 653–660.

Mischel, M., Seelig, J., Braganza, L. F., & Büldt, G. (1987) *Chem. Phys. Lipids 43*, 237–246.

Nabiev, I. R., Efremov, R. G., & Chumanov, G. D. (1985) *Proc. Int. Symp. Biomol. Struct. Interact., Suppl. J. Biosci.*, 363–374.

Otomo, J., Tomioka, A., Kinoshita, K., Miyata, H., Takenaka, Y., Kouyama, T., & Ikegami, A. (1988) *Biophys. J. 54*, 57–64.

Perutz, M. F. (1954) *Proc. R. Soc. London, A 225*, 264–286.

Renthal, R., & Cha, C. H. (1984) *Biophys. J. 45*, 1001–1006.

Seiff, F., Wallat, I., Ermann, P., & Heyn, M. P. (1985) *Proc. Natl. Acad. Sci. U.S.A. 82*, 3227–3231.

Seiff, F., Westerhausen, J., Wallat, I., & Heyn, M. P. (1986) *Proc. Natl. Acad. Sci. U.S.A. 83*, 7746–7750.

Tsetlin, V. I., Zakis, V. I., Aldashev, A. A., Kuryatov, A. B., Ovechkina, G. V., & Snyrov, V. L. (1983) *Bioorg. Khim. 9*, 1589–1605.

Worcester, D. L. (1975) Neutron scattering for the analysis of biological structures, *Brookhaven Symp. Biol. 27*, III-37–57.

Zaccai, G., & Gilmore, D. J. (1979) *J. Mol. Biol. 132*, 181–191.